agronomy

MDPI

Article

UAV Multispectral Imagery Combined with Canopy Vertical Layering Information for Leaf Nitrogen Content Inversion in Cotton

Kaixuan Li, Chunqi Yin, Yangbo Ye, Xueya Han and Sanmin Sun *

Modern Agricultural Engineering Key Laboratory at Universities of Education Department of Xinjiang Uygur Autonomous Region, College of Water Hydraulic and Architectural Engineering, Tarim University, Alar 843300, China; likaixuan003@163.com (K.L.); ycq00708@163.com (C.Y.); yyb231@163.com (Y.Y.); hanxueya0@163.com (X.H.)

* Correspondence: ssmaqx@126.com

Abstract

Leaf nitrogen concentration (LNC) exhibits pronounced vertical heterogeneity across canopy layers, which affects the accuracy of nitrogen diagnosis derived from UAV-based remote sensing imagery. To address the differential contributions of leaf nitrogen from distinct canopy strata and the limitations associated with single-source features, this study proposes an integrated framework that combines cumulative LNC indicators across canopy layers with multi-source feature sets (vegetation indices and texture features). Centered on three core technical innovations—(1) incorporating canopy-layer aggregation logic into LNC modeling, (2) integrating spectral and structural information through CNN-based feature fusion, and (3) combining deep feature extraction with gradient boosting regression to improve robustness under multi-stage conditions—the framework systematically evaluates three machine learning algorithms: Random Forest (RF), a Convolutional Neural Network–Extreme Gradient Boosting hybrid model (CNN_XGBoost), and K-Nearest Neighbor (KNN) for cotton LNC estimation across multiple growth stages. The results demonstrate that cumulative canopy-layer nitrogen indicators more effectively represent overall plant nitrogen status than single-layer measurements. The integration of multi-source features further enhances model performance. Under both single-variable inputs and combined VI–TF feature sets, the CNN_XGBoost model consistently outperforms the other models in calibration accuracy and stability across all growth stages. Its optimal performance occurs during the cotton flowering and boll stage, achieving a calibration R^2 of 0.921. Overall, the proposed framework substantially improves the estimation accuracy of cotton LNC and provides both a theoretical foundation and technical support for precision nitrogen management and sustainable agricultural development.

Keywords: cotton; leaf nitrogen content; multi-source features; machine learning

Check for updates

Received: 24 January 2026
Revised: 4 March 2026
Accepted: 7 March 2026
Published: 12 March 2026

Copyright: © 2026 by the authors. Licensee MDPI, Basel, Switzerland. This article is an open access article distributed under the terms and conditions of the Creative Commons Attribution (CC BY) license.

1. Introduction

Cotton is one of the world's most important fiber crops, accounting for approximately 35% of global fiber production and 49% of total fiber utilization [1]. In addition to its economic value as a textile raw material, cottonseed provides a rich source of essential amino acids (EAAs), such as methionine and leucine, which have high nutritional value [2]. Therefore, achieving high and stable cotton yields is critical for global economic stability, food security, and overall quality of life [3].

Nitrogen is a key nutrient in crop production, regulating plant growth dynamics, biomass accumulation, photosynthesis, protein synthesis, and carbon–nitrogen metabolism [4–8]. Timely and accurate assessment of crop nitrogen status can guide precision fertilization strategies and prevent environmental pollution caused by excessive nitrogen application. Conversely, nitrogen deficiency leads to leaf chlorosis, reduced photosynthetic capacity, and stunted growth, ultimately decreasing yield. Therefore, rapid and reliable monitoring of leaf nitrogen content in cotton, combined with rational nutrient management, is essential for ensuring both yield and quality.

Traditional methods for determining nitrogen content in cotton leaves, such as the Kjeldahl method and the Dumas combustion method [9], are destructive, labor-intensive, and time-consuming. With advances in remote sensing technology, satellite- and UAV-based platforms are increasingly used for rapid, non-destructive monitoring of crop growth indicators across spatial scales. For example, Lapaz Olveira et al. [10] demonstrated that integrating optical and C-SAR satellite data with soil nitrogen information improves dynamic nitrogen assessment in field corn. Li et al. [11] combined near-surface hyperspectral measurements with multi-source satellite simulations and found that visible, red-edge, near-infrared, and yellow-edge bands are critical for estimating nitrogen content in apple orchards. Among different satellite platforms, Sentinel-2 produced superior nitrogen inversion performance compared to Landsat-8 and GF-6.

However, compared with satellite remote sensing, UAV platforms equipped with multispectral sensors enable finer spatial resolution and more flexible operation, with reduced atmospheric interference. Matese et al. [12] demonstrated that UAV-based remote sensing provides higher resolution and greater accuracy than satellite platforms in precision viticulture applications. Despite these advances, most existing studies rely primarily on canopy-level spectral information and treat the canopy as a homogeneous unit. Such approaches often neglect vertical heterogeneity in nitrogen distribution and the associated structural–spectral interactions across canopy layers, thereby limiting the accuracy of leaf nitrogen estimation models.

Under nitrogen-deficient conditions, lower canopy leaves typically exhibit chlorosis first due to shading and senescence, whereas middle canopy leaves serve as a transitional zone linking nutrient redistribution and photosynthetic function. Upper leaves maintain higher photosynthetic activity through preferential nitrogen allocation [13]. Pan et al. [14] demonstrated that maize canopies exhibit pronounced vertical heterogeneity in light interception, physiological activity, and nitrogen distribution, which significantly influences the relationship between leaf nitrogen content and canopy spectral responses, thereby affecting diagnostic accuracy. Traditional canopy-based LNC models generally treat the canopy as a homogeneous unit and ignore its vertical heterogeneity, which may reduce the stability of estimation.

To address this issue, this study adopts a stratified sampling strategy with progressive integration of canopy-layer information. Specifically, upper leaves, upper plus middle layers, and the entire canopy were analyzed separately to quantify the marginal contribution of each layer and to test the "redundancy–complementarity" hypothesis [15]. This hypothesis examines whether incorporating intermediate canopy layers enhances model performance while minimizing redundant information.

Although stratified canopy analysis accounts for vertical nitrogen heterogeneity, traditional single-source spectral indices remain insufficient for accurate nitrogen diagnosis. In contrast, texture features (TFs) effectively characterize spatial heterogeneity and structural variation within plant canopies. Therefore, this study integrates spectral vegetation indices (VIs) and texture features to exploit their complementary strengths, thereby enhancing the robustness and generalizability of canopy nitrogen estimation.

Furthermore, we target the vertical heterogeneity of leaf nitrogen concentration (LNC) across different cotton canopy layers and construct an estimation framework that integrates cumulative canopy nitrogen indicators, multispectral vegetation indices, and texture features. A CNN-XGBoost hybrid model is proposed to enhance both prediction accuracy and model stability throughout the entire cotton growth period. This framework differs from conventional UAV-based machine learning studies by explicitly incorporating canopy stratification logic and deep feature fusion into a single-target regression structure.

2. Materials and Methods

2.1. Description of the Test Site

The experiment was conducted at the Agricultural Academy Expert Workstation in Aral City, Xinjiang Uygur Autonomous Region, China (81.17° E, 40.32° N), as shown in Figure 1. The region is characterized by a typical warm temperate continental arid desert climate, with low annual precipitation, extended sunshine duration, and high evaporation rates. The experimental soil is sandy in texture, and its fundamental physicochemical properties are summarized in Table 1.

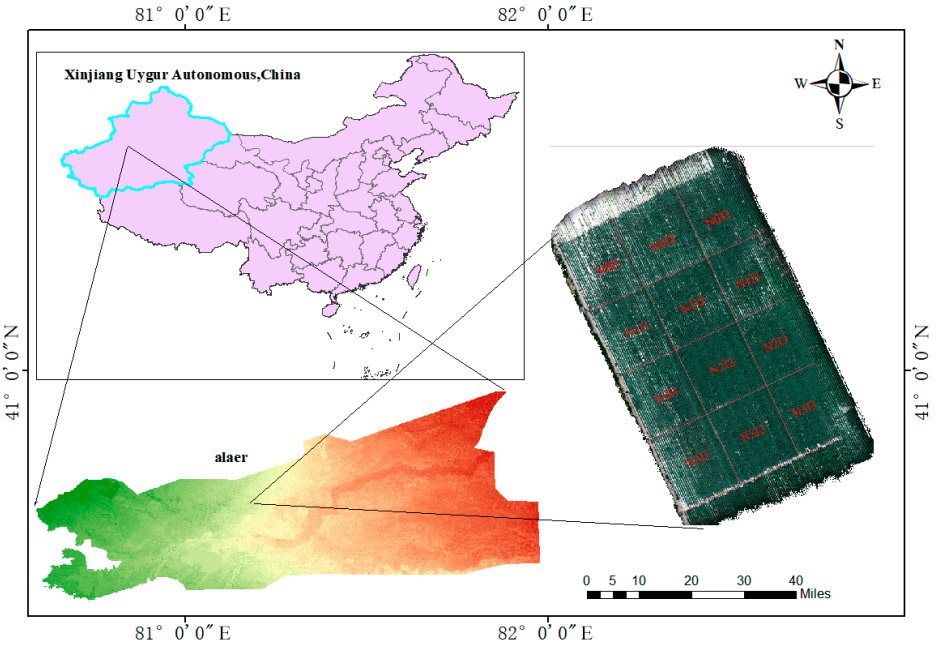


Figure 1. Overview Map of the Study Area.

Table 1. Soil Nutrient Content Parameters.

Soil Depth cm	Total Nitrogen Content mg·g^{-1}	Total Phosphorus Content mg·g^{-1}	Total Potassium Content mg·g^{-1}	Organic Matter mg·g^{-1}
0~10	0.025	0.75	20.4	3.19
10~20	0.028	0.79	19.5	3.58
20~40	0.033	0.95	19.3	2.85
40~60	0.022	0.43	19.7	2.50

2.2. Experimental Design

The cotton cultivar "Tahe No. 2" was selected as the experimental material. During the growing season, the irrigation quota was set at 375 m^3·hm^{-2}, with three irrigation treatments: 0.8 × (I1), 1.0 × (I2), and 1.2 × (I3) of the standard irrigation amount. Four nitrogen application levels were established: 0 kg·hm^{-2} (N0), 170 kg·hm^{-2} (N1),

340 kg·hm^{-2} (N2), and 510 kg·hm^{-2} (N3). Cotton was sown on 30 April 2023. A total of 12 experimental plots were arranged, each covering an area of 533 m^2. The planting configuration followed a "one film, three drip lines, and six rows" pattern with alternating wide and narrow row spacing (Figure 2).

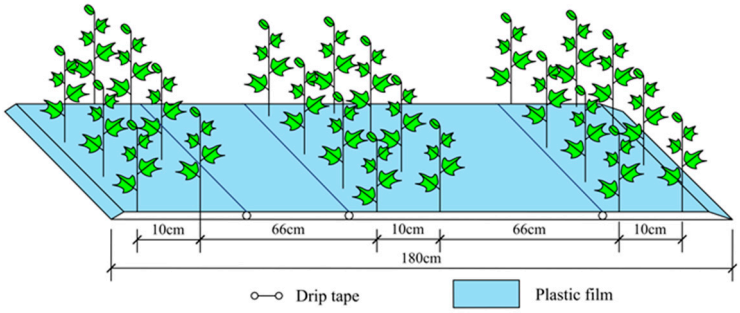


Figure 2. Cotton Planting Pattern.

Urea (N ≥ 46%) was used as the nitrogen fertilizer, monoammonium phosphate (P_2O_5 ≥ 60%) as the phosphorus fertilizer, and potassium sulfate (K_2O ≥ 52%) as the potassium fertilizer. All other agronomic management practices were implemented in accordance with local cultivation guidelines. The overall technical workflow of the experiment is illustrated in Figure 3.

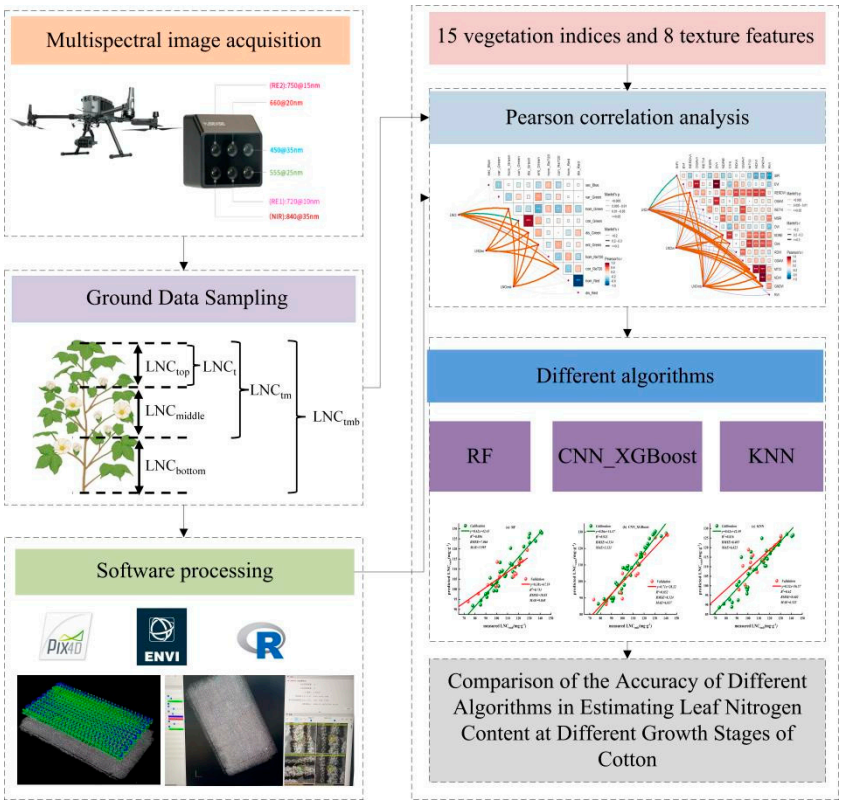


Figure 3. Technical Workflow of the Experiment.

2.3. Data Collection and Preprocessing

2.3.1. UAV Data Acquisition and Processing

UAV remote sensing data were collected using a DJI Matrice 350 RTK platform (DJI, Shenzhen, China) equipped with an MS600Pro multispectral camera. The camera integrates six spectral channels, each employing a 1.2 MP high-dynamic-range global shutter

CMOS sensor. The system captures five primary bands: blue, green, red, red edge, and near-infrared (NIR).

Data acquisition was conducted during four key phenological stages of cotton: late seedling stage, bud stage, boll stage, and boll-opening (fluffing) stage. Prior to each flight mission, reflectance measurements of a calibrated gray reference panel were obtained for radiometric correction. UAV flights were performed at a fixed altitude of 20 m and a constant speed of 2.8 $m \cdot s^{-1}$, with both forward and side overlaps set to 80%. All flights were conducted under clear, windless conditions between 13:00 and 14:00 Beijing Time (BT) to minimize illumination variability.

2.3.2. Ground Data Acquisition

Field sampling was conducted immediately after each UAV flight. In each plot, cotton plants with uniform growth were selected, and four representative leaves were collected from the upper, middle, and lower canopy layers. A total of 144 samples were collected at each growth stage, resulting in an overall dataset of 576 samples. The collected leaves were transported to the laboratory for determination of leaf nitrogen concentration (LNC). Of the total samples, 70% were randomly assigned to the training set for model development, and the remaining 30% were reserved as an independent test set for model validation.

2.3.3. Spectral Data Preprocessing

Image mosaicking, geometric correction, and radiometric calibration were performed using Pix4Dmapper (Pix4D, Prilly, Switzerland). Atmospheric correction and region-of-interest (ROI) extraction were subsequently conducted in ENVI 5.3.1 software to eliminate interference from soil background and plastic mulch shadows. Mean canopy reflectance values were calculated for each plot. Based on these reflectance data, 15 vegetation indices (VIs) associated with cotton nitrogen status were computed to quantitatively characterize canopy structure and growth (Table 2).

Table 2. Vegetation Indices Used in This Study.

Vegetation Index	Formula	References
Normalized Difference Vegetation Index (NDVI)	$NDVI = (NIR - Red)/(NIR + Red)$	[16]
Green Normalized Difference Vegetation Index (GNDVI)	$GNDVI = (NIR - Green)/(NIR + Green)$	[17]
Ration Vegetation Index (RVI)	$RVI = NIR/Red$	[18]
Meris Terrestrial Chlorophyll Index (MTCI)	$MTCI = (NIR - RedEdge)/(RedEdge - Red)$	[19]
Structure-Insensitive Pigment Index (SIPI)	$SIPI = (NIR - Blue)/(NIR - Red)$	[20]
Enhanced Vegetation Index (EVI)	$EVI = G \times (NIR - Red)/(NIR + C_1 \times Red - C_2 \times Blue + L)$	[21]
Red Edge Renormalized Difference Vegetation Index (RERDVI)	$RERDVI = (NIR - RedEdge)/(NIR + RedEdge + 0.5)$	[22]
Optimized Soil-Adjusted Vegetation Index (OSAVI)	$OSAVI = (1 + 0.16) \times (NIR - Red)/(NIR + Red + 0.16)$	[23]
Red Edge Triangular Vegetation Index (RETVI)	$RETVI = 0.5 \times (120 \times NIR - Red) - 200 \times (RedEdge - Red)$	[24]
Modified Simple Ratio Index (MSRI)	$MSRI = ((NIR/Red) - 1)/(((NIR/Red) + 1)^{0.5})$	[25]
Difference Vegetation Index (DVI)	$DVI = NIR - Red$	[26]
Normalized Difference Red Edge Index (NDRE)	$NDRE = (NIR - RedEdge)/(NIR + RedEdge)$	[27]
Chlorophyll Index Red Edge (CI_{re})	$CI_{re} = NIR/RedEdge - 1$	[28]
Renormalized Difference Vegetation Index (RDVI)	$RDVI = (NIR - Red)/(NIR + Red)^{0.5}$	[29]
Green Soil Adjusted Vegetation Index (GSAVI)	$GSAVI = 1.16 \times (NIR - Green)/(NIR + Green + 0.16)$	[30]

To capture canopy structural heterogeneity related to nitrogen distribution, texture features (TFs) were extracted using the gray-level co-occurrence matrix (GLCM) method implemented in ENVI 5.3.1. Texture features were calculated for the blue, green, red, red-edge, and near-infrared bands. A 3 × 3 moving window and a 45° direction were adopted for GLCM computation. For each band, eight texture metrics were extracted: mean (mea), variance (var), entropy (ent), contrast (con), correlation (cor), second moment (sem), homogeneity (hom), and dissimilarity (dis).

2.3.4. Determination of Nitrogen Content in Cotton Leaves

Collected leaf samples were initially heated at 105 °C for 30 min to deactivate enzymatic activity, followed by oven drying at 80 °C for 48 h to achieve constant weight. The dried samples were then finely ground using a mortar and pestle. Approximately 15 mg of the powdered material was weighed and sealed in a tin capsule for analysis. Leaf nitrogen concentration was determined using an elemental analyzer (Vario Isotope Cube, Elementar, Langenselbold, Germany).

2.4. Model Building and Evaluation

2.4.1. Feature Selection and Canopy Fusion

To improve the accuracy of cotton leaf nitrogen concentration (LNC) prediction, a multi-source feature fusion strategy was adopted. A total of 15 vegetation indices (VIs) and 8 texture features (TFs) were integrated as input variables for model inversion. The nitrogen contents of three canopy configurations—upper leaves (LNCt), upper plus middle leaves (LNCtm), and upper plus middle plus bottom leaves (LNCtmb)—were treated as dependent variables. These features jointly capture the multidimensional spectral characteristics and spatial structural attributes of the cotton canopy, enabling a more comprehensive representation of nitrogen distribution and thereby improving inversion accuracy.

2.4.2. Machine Learning Models

Using different canopy-layer nitrogen combinations as dependent variables and various feature combinations as independent variables, relationships between multi-source features and canopy nitrogen indicators were established using three machine learning algorithms: Random Forest (RF), a Convolutional Neural Network–Extreme Gradient Boosting hybrid model (CNN_XGBoost), and K-Nearest Neighbors (KNNs). These models represent ensemble learning, deep learning, and classical distance-based learning approaches, respectively. All models were implemented in RStudio 4.5.1, with the random seed fixed at 123 to ensure reproducibility.

RF, a representative ensemble learning method, enhances model accuracy and robustness by constructing multiple decision trees and aggregating their predictions. Because each tree is trained on randomly sampled data and feature subsets, RF reduces model variance and improves generalization performance [31]. In this study, the randomForest package was used for regression modeling, the caret package for data partitioning and performance evaluation, and ggplot2 for visualization.

The CNN_XGBoost hybrid model first performs automatic feature extraction using a convolutional neural network (CNN), and subsequently feeds the extracted deep features into an XGBoost regressor for prediction. The CNN component was implemented using the keras package to construct the feature extraction network, while the xgboost package was used to perform gradient boosting regression. The K-Nearest Neighbors (KNN) algorithm predicts target values by calculating the distance between a query sample and all samples in the training set, selecting the K nearest neighbors, and aggregating their corresponding outputs.

To control model complexity and mitigate overfitting, regularization strategies were implemented. In XGBoost, the maximum tree depth was limited to two layers to prevent the model from fitting minor fluctuations in vegetation indices and texture features. A relatively low learning rate (0.05) was adopted to ensure gradual optimization, and a high minimum child weight (6) was set to penalize extreme fitting to small subsets of samples. The CNN architecture consisted of two convolutional layers, two pooling layers, and two fully connected layers. The first fully connected layer included 128 neurons with a dropout

rate of 0.3 to reduce overfitting. The second fully connected layer contained 23 neurons, corresponding to the dimensionality of the fused input features.

Additionally, row subsampling (subsample = 0.7) and column subsampling (colsample_bytree = 0.6) were applied to randomly sample training observations and feature subsets. These strategies reduced redundancy among high-dimensional predictors (e.g., vegetation indices and GLCM-derived texture metrics) and enhanced generalization performance. Rather than manually tuning hyperparameters, a five-fold cross-validation procedure was conducted to systematically identify the optimal parameter combination, thereby ensuring statistical rigor and reproducibility.

2.4.3. Model Evaluation

Model performance and stability in predicting cotton leaf nitrogen concentration were evaluated using the coefficient of determination (R^2), root mean square error (RMSE), and mean absolute error (MAE). The corresponding formulas are as follows:

$$R^2 = 1 - \frac{\sum_{i=1}^{n}(M_i - S_i)^2}{\sum_{i=1}^{n}(M_i - \overline{M})^2} \quad (1)$$

$$RMSE = \sqrt{\frac{\sum_{i=1}^{n}(M_i - S_i)^2}{n}} \quad (2)$$

$$MAE = \frac{1}{n}\sum_{i=1}^{n}|M_i - S_i| \quad (3)$$

where M_i represents the measured value, S_i denotes the predicted value, $\overline{M}$ is the mean of the measured values, and n is the total number of samples used in the error calculation.

3. Results

3.1. Temporal Dynamics of Nitrogen Distribution in Cotton Canopy

The cloud–rain plots illustrate the dynamic distribution of leaf nitrogen concentration (LNC) across different growth stages and canopy-layer combinations (Figure 4). In these plots, the vertical axis represents different canopy-layer configurations, while the horizontal axis denotes LNC values. Overall, LNC increased during early development, reaching its peak at the flowering (boll) stage, with an average value of 108.1 $g \cdot kg^{-1}$, and subsequently declined to its lowest level at the boll-opening (fluffing) stage, with an average of 71.9 $g \cdot kg^{-1}$.

In the above figure, LNC_t represents nitrogen content in upper canopy leaves; LNC_{tm}, cumulative nitrogen content in upper and middle canopy leaves; and LNC_{tmb}, cumulative nitrogen content in upper, middle, and lower canopy leaves. Panels a–d represent the seeding, bud, boll, and fluffing stages, respectively. The same notation applies below.

3.2. Correlation Analysis

Correlation analyses were conducted between the three LNC metrics (LNC_t, LNC_{tm}, LNC_{tmb}) and vegetation indices (VIs) across four growth stages (Figure 5).

Seeding stage (Figure 5a): All LNC metrics were positively correlated with VIs, with correlation coefficients ranging from 0.54–0.72 (LNC_t), 0.50–0.74 (LNC_{tm}), and 0.50–0.75 (LNC_{tmb}). The strongest correlations were observed with RETVI, CIre, MTCI, NDVI, and GNDVI, with CIre showing the highest coefficients (0.72, 0.74, and 0.75, respectively). The highly consistent correlation patterns among LNC_t, LNC_{tm}, and LNC_{tmb} suggest similar spectral responses and regulatory mechanisms during early growth.

Bud stage (Figure 5b): Positive correlations remained dominant, with ranges of 0.73–0.82 (LNC_t), 0.71–0.79 (LNC_{tm}), and 0.68–0.75 (LNC_{tmb}). LNCt exhibited the strongest

associations, particularly with CIre (maximum coefficient of 0.82). A clear decreasing trend in correlation strength was observed as lower canopy layers were incorporated (LNC_t > LNC_{tm} > LNC_{tmb}).

Boll stage (Figure 5c): This stage exhibited the strongest overall correlations, with ranges of 0.54–0.82 (LNC_t), 0.53–0.83 (LNC_{tm}), and 0.50–0.78 (LNC_{tmb}). LNC_t and LNC_{tm} showed similar correlation patterns, particularly for RERDVI, MTCI, NDVI, and GNDVI (coefficients > 0.80). Incorporation of lower canopy layers reduced correlation strength.

Fluffing stage (Figure 5d): Correlation ranges narrowed to 0.71–0.75 (LNCt), 0.72–0.77 (LNCtm), and 0.72–0.76 (LNC_{tmb}), with minimal differences among canopy configurations. This stabilization may be attributed to canopy lodging and nitrogen remobilization from leaves to bolls, which homogenized spectral responses across layers.

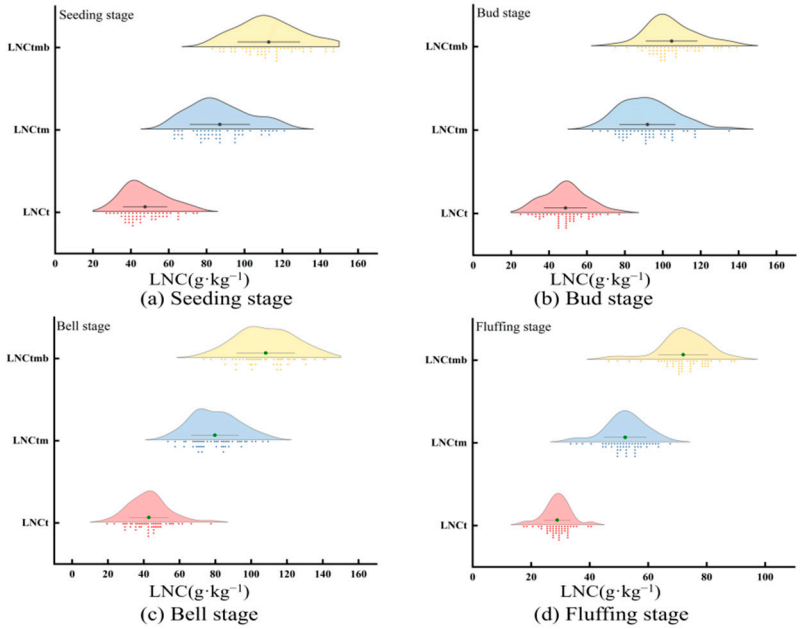


Figure 4. Distribution of Nitrogen Content Across Different Growth Stages.

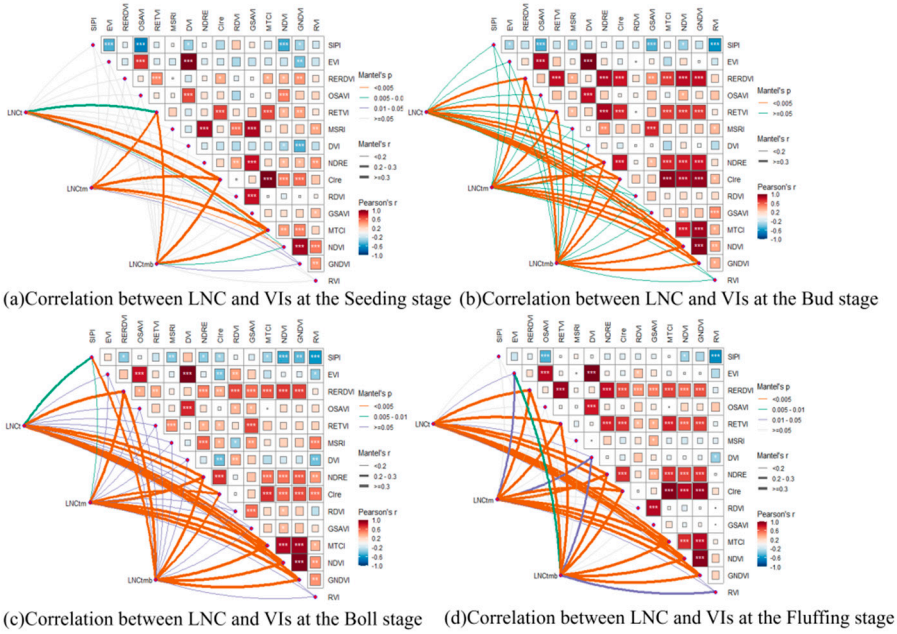
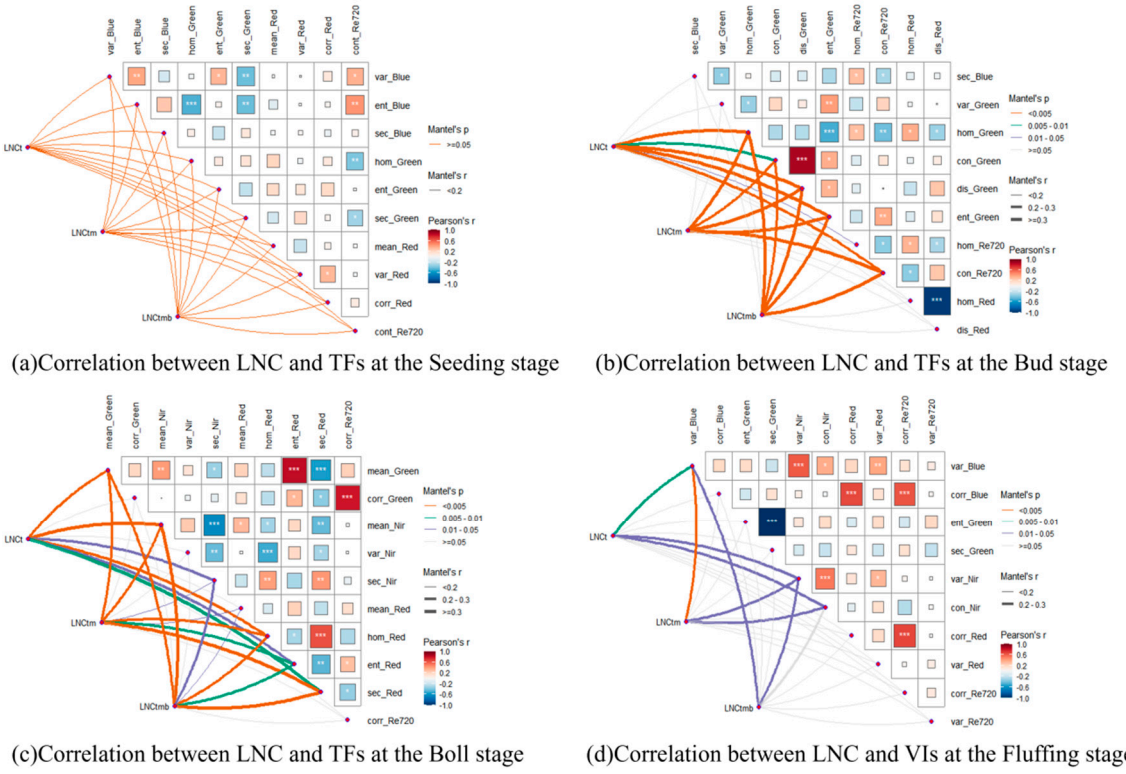


Figure 5. Correlation Between Canopy Leaf Nitrogen Metrics and Vegetation Indices. * $p \leq 0.05$, ** $p \leq 0.01$, and *** $p \leq 0.001$.

Correlation analyses were also conducted between LNC metrics and texture features (TFs), with the highest-ranking TFs (by correlation coefficient) retained for each stage (Figure 6).



(a)Correlation between LNC and TFs at the Seeding stage (b)Correlation between LNC and TFs at the Bud stage

(c)Correlation between LNC and TFs at the Boll stage (d)Correlation between LNC and VIs at the Fluffing stage

Figure 6. Correlation Between Canopy Leaf Nitrogen Metrics and Texture Features. * $p \leq 0.05$, ** $p \leq 0.01$, and *** $p \leq 0.001$.

Seeding stage (Figure 6a): All correlations were positive, ranging from 0.42–0.47 (LNC_t), 0.32–0.49 (LNC_{tm}), and 0.45–0.48 (LNC_{tmb}). The strongest correlations were observed for LNC_t with var_Blue (0.47), ent_Green (0.43) and var_Red (0.42); for LNC_{tm} with var_Blue (0.49), ent_Green (0.43), var_Red (0.39) and corr_Red (0.32); and for LNCtmb with var_Blue (0.48), ent_Green (0.44), var_Red (0.45) and corr_Red (0.32). Correlation patterns were highly consistent across canopy configurations.

Bud stage (Figure 6b): Both positive and negative correlations were observed, with coefficients ranging from −0.80–0.64 (LNC_t), −0.77–0.63 (LNC_{tm}) and −0.65–0.60 (LNC_{tmb}). The most responsive TFs for LNC_t included var_Green (0.40), hom_Green (−0.80), ent_Green (0.64), hom_Re720 (−0.36), con_Re720 (0.62), hom_Red (−0.34) and dis_Red (0.33); for LNC_{tm} included var_Green (0.41), hom_Green (−0.77), ent_Green (0.63), hom_Re720 (−0.31) and con_Re720 (0.60); and for LNCtmb included var_Green (0.40), hom_Green (−0.65), ent_Green (0.60), hom_Re720 (−0.30) and con_Re720 (0.58). Strong negative correlations were detected for hom_Green, while var_Green and ent_Green exhibited positive associations. Correlation strength slightly decreased when lower canopy layers were included.

Boll stage (Figure 6c): Correlation coefficients ranged from −0.49–0.58 (LNC_t), −0.51–0.59 (LNC_{tm}) and −0.53–0.60 (LNC_{tmb}). In contrast to the bud stage, correlation strength slightly increased when cumulative canopy layers were considered. Key TFs included mean_Green (0.54), man_Nir (0.58), var_Nir (0.32), sec_Nir (−0.43), hom_Red (−0.42), ent_Red (0.40) and sec_Red (−0.49); for LNC_{tm} were mean_Green (0.49), man_Nir (0.59), var_Nir (0.31), sec_Nir (−0.42), hom_Red (−0.43), ent_Red (0.37) and sec_Red

(−0.51); and for LNC_{tmb} were mean_Green (0.51), man_Nir (0.60), var_Nir (0.33), sec_Nir (−0.43), hom_Red (−0.43), ent_Red (0.39) and sec_Red (−0.53).

Fluffing stage (Figure 6d): Correlation ranges were −0.35–0.67 (LNC_t), −0.37–0.68 (LNC_{tm}) and −0.39–0.66 (LNC_{tmb}). The correlation structure stabilized across canopy configurations. The most strongly associated TFs were var_Blue, ent_Green, sec_Green, var_Nir, con_Nir and var_Red across all LNC metrics, with var_Blue achieving the highest coefficients (0.67 for LNC_t, 0.68 for LNC_{tm}, 0.66 for LNC_{tmb}).

Overall, LNC_{tmb} demonstrated consistently strong correlations with both VIs and TFs. Therefore, LNC_{tmb} was selected as the target variable for subsequent modeling.

3.3. Establishment and Evaluation of LNC Estimation Models

Based on correlation analysis and variable importance (Figure 7), stage-specific feature subsets were selected as model inputs (Table 3). Evaluation models were constructed using random forest (RF), convolutional neural network-XGBoost (CNN_XGBoost), and KNN, with their performance summarized in Table 4.

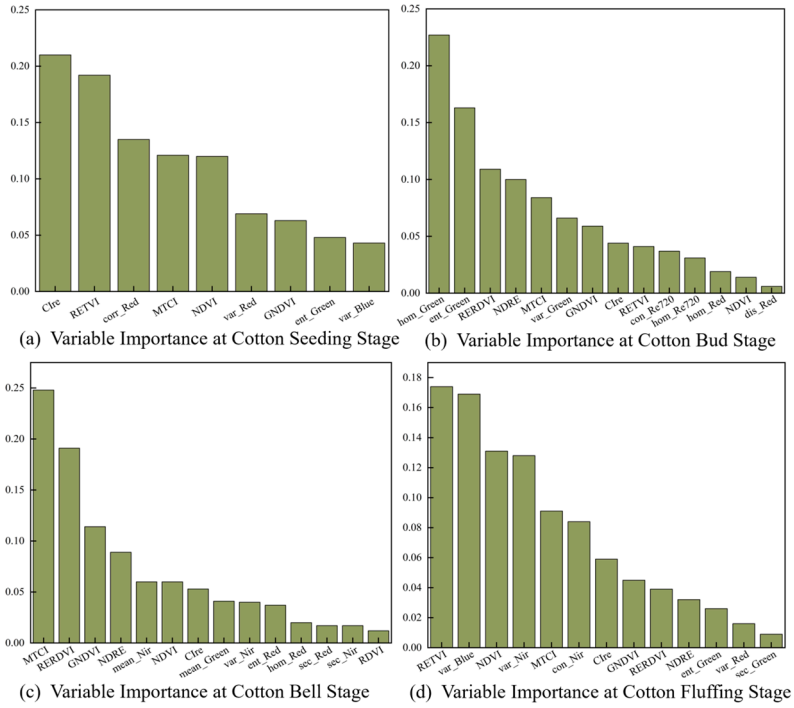


Figure 7. Variable importance.

Table 3. Model Input Variable Selection.

Growth Period	Input Variable	Independent Variable
Seeding stage	VIs	RETVI, CI_{re}, MTCI, NDVI, GNVI
	TFs	var_Blue, ent_Green, var_Red, corr_Red
Bud stage	VIs	RERDVI, RETVI, NDRE, CI_{re}, MTCI, NDVI, GNVI
	TFs	var_Green, hom_Green, ent_Green, hom_Re720, con_Re720, hom_Red, dis_Red
Bell stage	VIs	RERDVI, NDRE, CI_{re}, MTCI, NDVI, GNVI
	TFs	mean_Green, man_Nir, var_Nir, sec_Nir, hom_Red, ent_Red, sec_Red
Fluffing stage	VIs	RERDVI, RETVI, NDRE, CI_{re}, MTCI, NDVI, GNVI
	TFs	var_Blue, ent_Green, sec_Green, var_Nir, con_Nir, var_Red

Table 4. Statistical Performance of Calibration and Validation for Cotton at Various Growth Stages under Different Modeling Approaches.

Growth Period	Input Variable	Modeling Method	Calibration			Validation		
			R^2	*RMSE*	*MAE*	R^2	*RMSE*	*MAE*
Seeding stage	VIs	RF	0.75	9.085	7.149	0.699	10.316	8.88
		CNN_XGBoost	0.81	8.4	6.238	0.78	6.975	5.838
		KNN	0.582	10.724	8.57	0.579	14.751	12.14
	TFs	RF	0.729	9.557	7.435	0.645	12.57	9.443
		CNN_XGBoost	0.727	9.043	7.425	0.716	9.012	7.58
		KNN	0.51	12.495	10.327	0.503	12.761	9.946
	VIs + TFs	RF	0.78	9.466	7.554	0.724	10.017	7.749
		CNN_XGBoost	0.821	6.911	5.662	0.784	11.478	8.167
		KNN	0.589	12.109	9.667	0.578	9.498	7.984
Bud stage	VIs	RF	0.838	6.336	4.763	0.659	8.703	7.117
		CNN_XGBoost	0.84	5.798	3.882	0.801	6.819	4.823
		KNN	0.639	8.954	6.666	0.588	9.065	6.95
	TFs	RF	0.798	8.14	5.994	0.791	8.092	6.56
		CNN_XGBoost	0.826	6.368	4.404	0.812	5.643	4.36
		KNN	0.664	10.002	7.478	0.656	9.32	7.262
	VIs + TFs	RF	0.886	6.285	4.47	0.764	8.555	7.27
		CNN_XGBoost	0.878	5.111	2.957	0.874	5.817	5.057
		KNN	0.712	8.926	6.454	0.607	7.419	6.226
Bell stage	VIs	RF	0.86	6.393	5.637	0.742	11.545	9.175
		CNN_XGBoost	0.889	5.334	4.205	0.854	7.182	5.818
		KNN	0.8	8.19	6.559	0.655	7.464	6.161
	TFs	RF	0.735	9.817	8.525	0.728	10.951	9.937
		CNN_XGBoost	0.786	7.565	5.917	0.759	8.988	6.4
		KNN	0.522	11.963	10.858	0.446	14.389	11.829
	VIs + TFs	RF	0.886	7.066	5.995	0.751	10.83	9.848
		CNN_XGBoost	0.921	4.334	3.321	0.852	8.124	6.837
		KNN	0.816	8.405	6.623	0.62	8.602	6.523
Fluffing stage	VIs	RF	0.826	3.494	2.543	0.773	5.675	4.133
		CNN_XGBoost	0.796	3.898	2.789	0.791	4.184	3.461
		KNN	0.62	5.34	4.105	0.601	5.661	4.781
	TFs	RF	0.804	3.527	2.391	0.739	3.618	2.93
		CNN_XGBoost	0.816	3.475	2.335	0.81	4.943	3.727
		KNN	0.632	5.044	2.838	0.606	7.161	4.553
	VIs + TFs	RF	0.816	3.288	2.445	0.699	2.885	2.556
		CNN_XGBoost	0.853	3.307	2.148	0.836	3.76	3.128
		KNN	0.664	5.164	3.58	0.595	5.947	4.091

Overall, as shown in Table 4, both the selection of the modeling algorithm and the configuration of input variables substantially influence predictive performance, with clear discrepancies observed between the calibration and validation sets. Across all cotton growth stages, models incorporating combined vegetation indices (VIs) and texture features (TFs) consistently yield higher R^2 values than single-source inputs, indicating that multi-source integration enhances robustness and generalization capacity.

Under different feature configurations, the CNN_XGBoost model consistently achieves higher R^2 values than the Random Forest (RF) and K-Nearest Neighbor (KNN) models in both calibration and validation phases. During the bud stage, however, when VIs and TFs are combined, the calibration R^2 of CNN_XGBoost is 0.9% lower than that of RF, although its overall stability remains superior. In the flowering (boll) stage, CNN_XGBoost demonstrates optimal performance, achieving a calibration R^2 of 0.921. In contrast, during the fluffing stage, RF exhibits the greatest stability in both calibration and validation sets,

with RMSE values of 3.288 and 2.885 and MAE values of 2.445 and 2.556, respectively. Across all stages and input configurations, KNN consistently shows lower predictive accuracy and weaker stability than both RF and CNN_XGBoost.

According to Table 4 and Figure 8, during the seeding stage, the CNN_XGBoost model with combined VI and TF inputs achieves the best overall performance. Its calibration R^2 increases by 12.93% relative to the best single-variable model, while RMSE and MAE decrease by up to 23.58% and 23.74%, respectively, indicating markedly improved fitting performance. In the validation set, the combined-input model attains the highest R^2 (0.784), representing a 9.5% improvement over the optimal single-variable model. However, compared with the model using only VIs, validation RMSE and MAE increase by 60.26% and 39.89%, respectively, suggesting reduced generalization stability.

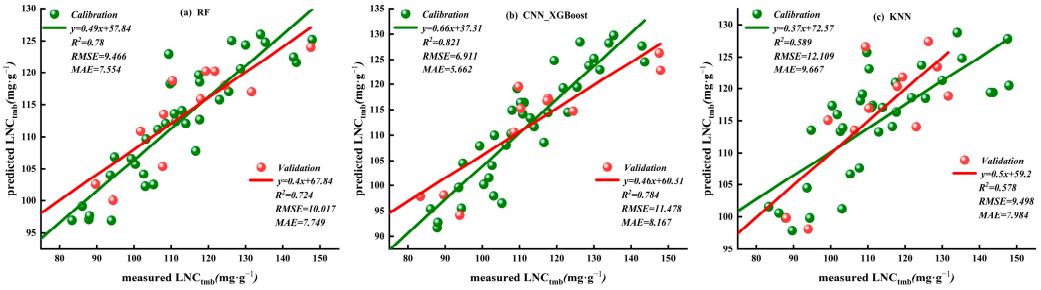


Figure 8. Scatter Plots of Measured versus Predicted LNC Values for Different Machine Learning Models during the Cotton Seeding Stage.

During the bud stage (Table 4 and Figure 9), the CNN_XGBoost model with combined inputs again achieves the highest calibration R^2, improving by 6.29% over the best single-variable model. Maximum reductions in RMSE and MAE reach 19.74% and 32.86%, respectively. In the validation set, the combined-input model attains a peak R^2 of 0.874, reflecting a 9.11% improvement relative to the best single-variable configuration. Nevertheless, compared with the single-TF model, validation RMSE and MAE increase by 3.08% and 15.99%, indicating a moderate decline in stability.

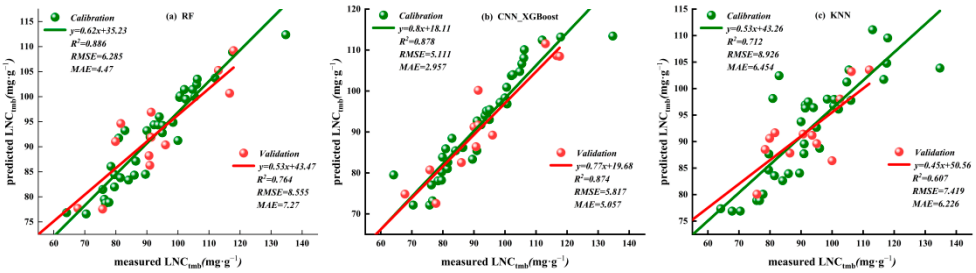


Figure 9. Scatter Plots of Measured versus Predicted LNC Values for Different Machine Learning Models during the Cotton Bud Stage.

During the flowering (boll) stage (Table 4 and Figure 10), the CNN_XGBoost model with combined inputs achieves the strongest calibration performance, with an R^2 of 0.921—an improvement of 17.18% over the best single-variable model. RMSE and MAE decrease by up to 42.71% and 43.87%, respectively, demonstrating excellent calibration performance. In the validation set, the combined-input model reaches an R^2 of 0.784, representing a 9.5% improvement over the best single-variable model. However, compared with the single-VI model, validation RMSE and MAE increase by 60.26% and 39.89%, respectively, indicating diminished generalization. Notably, among the single-VI validation models, RF achieves the highest R^2 (0.854), with corresponding RMSE and MAE values of 7.184 and 5.818, respectively.

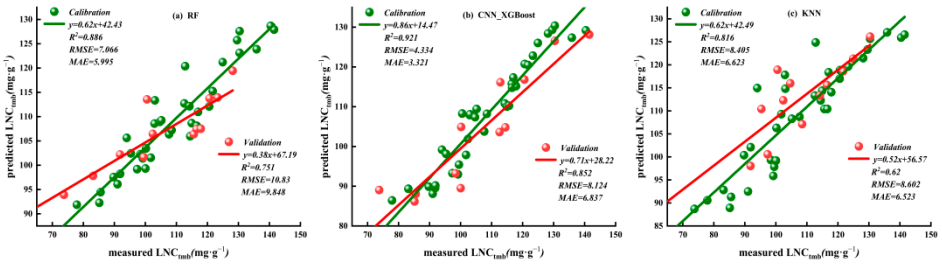


Figure 10. Scatter Plots of Measured versus Predicted LNC Values for Different Machine Learning Models during the Cotton Boll Stage.

During the fluffing stage (Table 4 and Figure 11), the CNN_XGBoost model with combined inputs again produces the highest calibration R^2, improving by 7.16% relative to the best single-variable model. RMSE and MAE decrease by up to 4.83% and 22.98%, respectively. In the validation set, the maximum R^2 reaches 0.836, representing a 5.69% improvement over the best single-variable model. However, compared with the RF model using single TF inputs, validation RMSE and MAE increase by 3.92% and 6.76%, respectively, suggesting reduced stability.

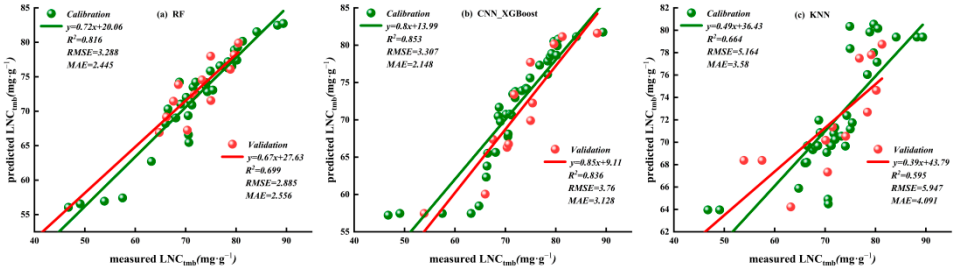


Figure 11. Scatter Plots of Measured versus Predicted LNC Values for Different Machine Learning Models during the Cotton Fluffing Stage.

In summary, irrespective of whether single-source or combined VI–TF inputs are used, CNN_XGBoost consistently demonstrates superior calibration accuracy across growth stages compared with RF and KNN. However, increases in validation RMSE and MAE without corresponding gains in R^2 indicate compromised generalization performance. These findings suggest that although the complementarity between spectral and textural features enhances calibration fitting, measurement noise and multicollinearity may adversely affect model stability in independent validation datasets.

4. Discussion

4.1. Determine the Trend of Nitrogen Content Concentration in Leaves

The upper and middle canopy layers constitute the main photosynthetic functional structure of cotton. The upper layer reflects real-time nitrogen nutrition, while the middle layer represents the main biomass and physiological activity. Their combination can more comprehensively reflect the actual nitrogen status of the plant, thus effectively improving the performance of the LNC estimation model.

LNC is a key indicator of the nitrogen nutritional status of crops. Figure 12 presents the variation in LNC under different irrigation and nitrogen application treatments. The results show a consistent increase in LNC with increasing levels of nitrogen fertilizer and irrigation. Under nitrogen treatments, the mean LNC values were 34.24 mg·g^{-1} (N0), 36.98 mg·g^{-1} (N1), 39.95 mg·g^{-1} (N2), and 40.38 mg·g^{-1} (N3), indicating a progressive enhancement in leaf nitrogen accumulation as nitrogen supply increased. Although the increment between N2 and N3 was relatively small, the overall upward trend confirms the

positive response of cotton leaf nitrogen status to nitrogen fertilization. Similarly, under irrigation treatments, LNC ranged from 33.33 to 38.90 mg·g^{-1} (I1), 33.90 to 40.84 mg·g^{-1} (I2), and 35.47 to 41.39 mg·g^{-1} (I3). These results suggest that increased water availability promotes nitrogen uptake and assimilation, likely by enhancing root activity and nutrient transport efficiency. This trend is consistent with the findings of Kou et al. [32], who reported significant variations in cotton leaf nitrogen content across different cultivars and nitrogen application gradients.

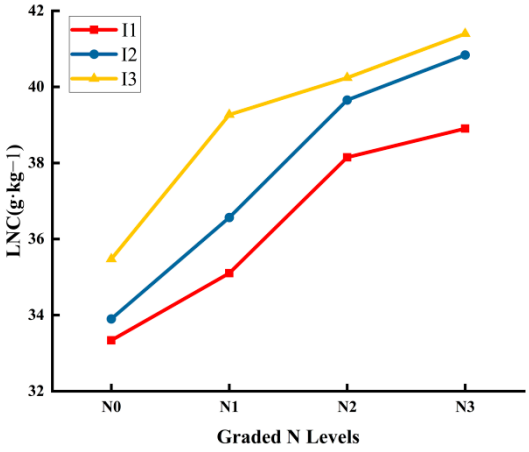


Figure 12. Changes in LNC under Different Irrigation and Nitrogen Treatments.

4.2. The Impact of Feature Selection on LNC Estimation Accuracy

This study identified key features at different cotton growth stages that are closely associated with the crop's nitrogen status, using correlation thresholds. Existing research indicates that a combination of vegetation indices (VIs) such as RERDVI, NDRE, CIre, MTCI, NDVI, and GNVI, together with texture features (TFs), can effectively reflect leaf nitrogen content and overall plant growth. At the vegetation index level, Han et al. [33] selected nine VIs based on previous studies to monitor the LNC of winter wheat using UAV multispectral data. Similarly, Zhou et al. [34] demonstrated that in cotton nitrogen estimation using multi-angle hyperspectral data, the correlation of spectral indices such as SIPI, GNDVI, and MTCI with actual nitrogen content varies significantly.

Regarding texture features, Li et al. [35] showed that multi-source features derived from multispectral images can enhance the robustness and accuracy of corn LAI estimation. Wen et al. [15] applied canopy stratification and multi-source remote sensing to diagnose corn nitrogen status, revealing that combining upper and middle canopy leaves provides a better representation of overall nitrogen levels. These findings support the scientific rationale and effectiveness of the multi-source feature combinations and layered canopy approach employed in this study.

Furthermore, Silva et al. [36] demonstrated that combining VIs and TFs significantly outperforms single indicators during the R7 growth stage of common bean, as well as throughout the growing season. Multi-source feature fusion, integrating VIs, TFs, and texture indices, provides a comprehensive representation of canopy nitrogen by combining spectral, textural, and structural information [36,37]. In this study, the synergistic use of 15 VIs and 8 TFs improved the performance of Random Forest (RF), Convolutional Neural Network with XGBoost (CNN_XGBoost), and K-Nearest Neighbors (KNN) models, enabling more accurate monitoring of the spatial structure and heterogeneity of the cotton canopy compared with single-source features, thereby enhancing the precision of cotton LNC estimation.

4.3. Impact of Machine Learning Models on LNC Estimation

The study evaluated cotton LNC across growth stages using three machine learning models. The results indicate that the CNN_XGBoost model generally outperforms the RF model in accuracy throughout the growth period, while the KNN model exhibits the lowest stability. Specifically, CNN_XGBoost achieved optimal performance during the cotton Bell stage, with R^2 values of 0.921 and 0.852 for calibration and validation sets, respectively, under the combined VIs and TFs input. Its stability, however, peaked during the Fluffing stage, with RMSE/MAE values of 3.307/3.760 (calibration) and 2.148/3.128 (validation). This is largely because CNN_XGBoost first extracts high-value features through CNN, followed by precise regression and classification using XGBoost. The RF model, an ensemble of decision trees, captures nonlinear relationships and is relatively robust to noise, reducing overfitting through aggregation. However, it relies on manual feature selection and cannot learn higher-order feature interactions, unlike CNN. In contrast, KNN depends solely on distance metrics and cannot model complex feature interactions.

Consistent with these findings, Xiao et al. [3] reported that XGBoost delivered the best predictive performance for cotton nitrogen nutrition indices, with R^2 approaching 100% and RMSE/MAE near zero. The ranking of model performance in their study was XGBoost > RF > KNN, with feature selection optimizing model stability. Hu et al. [38] similarly observed that KNN and SVR underperformed compared with RF in UAV hyperspectral inversion of spring wheat chlorophyll, aligning with the results of this study. Unlike prior studies focusing on traditional machine learning for canopy-based LNC prediction, CNN_XGBoost integrates deep learning and ensemble learning, leveraging complementary strengths in feature modeling to improve accuracy and robustness. Additionally, aggregating nitrogen content from upper, middle, and lower canopy layers enhances LNC inversion accuracy.

4.4. Future Research Directions

Although this study achieved promising results through CNN_XGBoost integration, these models may not represent the ultimate optimal solution. While CNN_XGBoost improves accuracy, its stability can be further enhanced. Moreover, although ground-based LNC measurements were aggregated across canopy layers, UAVs in this study were limited to capturing single-angle spectral data.

Future research could expand in the following directions: Firstly, integrating multi-angle spectral features for crop canopies to better characterize vertical canopy structure and overlapping effects; Secondly, exploring combinations of diverse machine learning models to further improve both accuracy and stability, building upon the complementary advantages demonstrated by CNN_XGBoost.

5. Conclusions

Using UAV-acquired multispectral data, we developed a spectral sensitivity index for cotton leaf nitrogen content (LNC) and combined it with texture features to construct predictive models. Nitrogen content values from different canopy layers were integrated as input variables, and three machine learning models were evaluated. Among these, the CNN_XGBoost model represents a novel approach that leverages both deep learning and ensemble learning. Based on the study results, the following main conclusions can be drawn:

(1) Significant differences exist among machine learning models in their ability to invert cotton LNC, highlighting the importance of model selection.

(2) Integrating nitrogen content from the upper, middle, and lower canopy leaves provides optimal input for LNC inversion. Additionally, combining spectral and texture information substantially improves model accuracy.

(3) The CNN_XGBoost model achieved the highest accuracy, reaching an R^2 of 0.921 during the cotton Bell stage; however, its stability requires further enhancement.

Overall, this study provides a robust framework for accurately estimating cotton LNC, offering valuable insights for precision management and optimization in cotton production.

Author Contributions: Conceptualization, K.L., C.Y., Y.Y., X.H. and S.S.; methodology, K.L. and S.S.; software, K.L. and S.S.; validation, K.L., C.Y., Y.Y. and X.H.; formal analysis, K.L., C.Y. and Y.Y.; investigation, K.L., C.Y., Y.Y. and X.H.; data curation, K.L. and S.S.; writing—original draft preparation, K.L. and S.S.; writing—review and editing, K.L. and S.S.; visualization, K.L. and S.S.; supervision, S.S.; project administration, S.S.; funding acquisition, S.S. All authors have read and agreed to the published version of the manuscript.

Funding: This study was supported by the earmarked fund for XJARS-Cotton (XJARS-03-17).

Data Availability Statement: The data presented in this study are available on request from the corresponding author; due to policy and legal reasons, data are classified and not disclosed.

Conflicts of Interest: The authors declare no conflicts of interest.

References

1. Abdelraheem, A.; Esmaeili, N.; O'Connell, M.; Zhang, J. Progress and Perspective on Drought and Salt Stress Tolerance in Cotton. *Ind. Crops Prod.* **2019**, *130*, 118–129. [CrossRef]
2. Li, Y.; Zou, J.; Zhu, H.; He, J.; Setter, T.L.; Wang, Y.; Meng, Y.; Chen, B.; Zhao, W.; Wang, S.; et al. Drought Deteriorated the Nutritional Quality of Cottonseed by Altering Fatty Acids and Amino Acids Compositions in Cultivars with Contrasting Drought Sensitivity. *Environ. Exp. Bot.* **2022**, *194*, 104747. [CrossRef]
3. Xiao, C.; Zhang, F.; Mäkelä, P.S.A.; He, J.; Fan, J.; Chen, J.; Li, Y.; Jiang, F.; Jia, Y. An Unmanned Aerial Vehicle-Based Cotton Nitrogen Nutrition Index Estimation Model Utilizing Feature Selection and Machine Learning. *Comput. Electron. Agric.* **2025**, *238*, 110798. [CrossRef]
4. Qiao, J.; Yang, L.; Yan, T.; Xue, F.; Zhao, D. Rice Dry Matter and Nitrogen Accumulation, Soil Mineral N around Root and N Leaching, with Increasing Application Rates of Fertilizer. *Eur. J. Agron.* **2013**, *49*, 93–103. [CrossRef]
5. Tahir Ata-Ul-Karim, S.; Liu, X.; Lu, Z.; Yuan, Z.; Zhu, Y.; Cao, W. In-Season Estimation of Rice Grain Yield Using Critical Nitrogen Dilution Curve. *Field Crops Res.* **2016**, *195*, 1–8. [CrossRef]
6. Li, S.; Ding, X.; Kuang, Q.; Ata-Ul-Karim, S.T.; Cheng, T.; Liu, X.; Tian, Y.; Zhu, Y.; Cao, W.; Cao, Q. Potential of UAV-Based Active Sensing for Monitoring Rice Leaf Nitrogen Status. *Front. Plant Sci.* **2018**, *9*, 1834. [CrossRef]
7. Vibhute, A.D.; Kale, K.V.; Gaikwad, S.V.; Dhumal, R.K. Estimation of Soil Nitrogen in Agricultural Regions by VNIR Reflectance Spectroscopy. *SN Appl. Sci.* **2020**, *2*, 1523. [CrossRef]
8. Zhuang, Y.; Wen, W.; Ruan, S.; Zhuang, F.; Xia, B.; Li, S.; Liu, H.; Du, Y.; Zhang, L. Real-Time Measurement of Total Nitrogen for Agricultural Runoff Based on Multiparameter Sensors and Intelligent Algorithms. *Water Res.* **2022**, *210*, 117992. [CrossRef]
9. Etheridge, R.D.; Pesti, G.M.; Foster, E.H. A Comparison of Nitrogen Values Obtained Utilizing the Kjeldahl Nitrogen and Dumas Combustion Methodologies (Leco CNS 2000) on Samples Typical of an Animal Nutrition Analytical Laboratory. *Anim. Feed Sci. Technol.* **1998**, *73*, 21–28. [CrossRef]
10. Lapaz Olveira, A.M.; Castro-Franco, M.; Saínz Rozas, H.R.; Carciochi, W.D.; Balzarini, M.; Avila, O.; Ciampitti, I.; Reussi Calvo, N.I. Monitoring Corn Nitrogen Nutrition Index from Optical and Synthetic Aperture Radar Satellite Data and Soil Available Nitrogen. *Precis. Agric.* **2023**, *24*, 2592–2606. [CrossRef]
11. Li, M.; Zhu, X.; Yu, X.; Li, C.; Xu, D.; Wang, L.; Lv, D.; Ma, Y. Nitrogen Content Estimation of Apple Trees Based on Simulated Satellite Remote Sensing Data. *Front. Plant Sci.* **2025**, *16*, 1613487. [CrossRef] [PubMed]
12. Matese, A.; Toscano, P.; Di Gennaro, S.; Genesio, L.; Vaccari, F.; Primicerio, J.; Belli, C.; Zaldei, A.; Bianconi, R.; Gioli, B. Intercomparison of UAV, Aircraft and Satellite Remote Sensing Platforms for Precision Viticulture. *Remote Sens.* **2015**, *7*, 2971–2990. [CrossRef]
13. Li, L.; Geng, S.; Lin, D.; Su, G.; Zhang, Y.; Chang, L.; Ji, Y.; Wang, Y.; Wang, L. Accurate Modeling of Vertical Leaf Nitrogen Distribution in Summer Maize Using in Situ Leaf Spectroscopy via CWT and PLS-Based Approaches. *Eur. J. Agron.* **2022**, *140*, 126607. [CrossRef]
14. Pan, Y.; Li, J.; Zhang, J.; He, J.; Zhang, Z.; Yao, X.; Cheng, T.; Zhu, Y.; Cao, W.; Tian, Y. Estimating Leaf Nitrogen Accumulation Considering Vertical Heterogeneity Using Multiangular Unmanned Aerial Vehicle Remote Sensing in Wheat. *Plant Phenomics* **2024**, *6*, 0276. [CrossRef]

15. Wen, L.; Yu, J.; Jiang, W.; Pei, S.; Liao, Z.; Zhang, F.; Fan, J.; Yin, F. Diagnosis of Maize Nitrogen Status under Contrasting Water and Nitrogen Regimes Using a Canopy-Stratified and Multi-Source Remote Sensing Framework. *Comput. Electron. Agric.* **2026**, *240*, 111148. [CrossRef]
16. Donovan, G.H.; Gatziolis, D.; Derrien, M.; Michael, Y.L.; Prestemon, J.P.; Douwes, J. Shortcomings of the Normalized Difference Vegetation Index as an Exposure Metric. *Nat. Plants* **2022**, *8*, 617–622. [CrossRef]
17. Gitelson, A.A.; Merzlyak, M.N. Remote Sensing of Chlorophyll Concentration in Higher Plant Leaves. *Adv. Space Res.* **1998**, *22*, 689–692. [CrossRef]
18. Jordan, C.F. Derivation of Leaf-Area Index from Quality of Light on the Forest Floor. *Ecology* **1969**, *50*, 663–666. [CrossRef]
19. Dash, J.; Curran, P.J. The MERIS Terrestrial Chlorophyll Index. *Int. J. Remote Sens.* **2004**, *25*, 5403–5413. [CrossRef]
20. Chen, Z.; Chen, Q.; Xu, H.G.; Huang, X.Q. Inversion model of summer maize plant height and biomass under different water and fertilizer treatments based on UAV spectra. *Agric. Res. Arid Area* **2023**, *41*, 198–207. (In Chinese with English Abstract)
21. Huete, A.; Didan, K.; Miura, T.; Rodriguez, E.P.; Gao, X.; Ferreira, L.G. Overview of the Radiometric and Biophysical Performance of the MODIS Vegetation Indices. *Remote Sens. Environ.* **2002**, *83*, 195–213. [CrossRef]
22. Wei, Q.; Zhang, B.Z.; Wei, Z.; Han, X.; Duan, C.F. Estimation of Canopy Chlorophyll Contentin Winter Wheat by UAV Multispectral Remote Sensing. *J. Triticeae Crops* **2020**, *40*, 365–372. (In Chinese with English Abstract) [CrossRef]
23. Rondeaux, G.; Steven, M.; Baret, F. Optimization of Soil-Adjusted Vegetation Indices. *Remote Sens. Environ.* **1996**, *55*, 95–107. [CrossRef]
24. Cao, Q.; Miao, Y.; Wang, H.; Huang, S.; Cheng, S.; Khosla, R.; Jiang, R. Non-Destructive Estimation of Rice Plant Nitrogen Status with Crop Circle Multispectral Active Canopy Sensor. *Field Crops Res.* **2013**, *154*, 133–144. [CrossRef]
25. Fan, X.; Gao, P.; Zhang, M.; Cang, H.; Zhang, L.; Zhang, Z.; Wang, J.; Lv, X.; Zhang, Q.; Ma, L. The Fusion of Vegetation Indices Increases the Accuracy of Cotton Leaf Area Prediction. *Front. Plant Sci.* **2024**, *15*, 1357193. [CrossRef]
26. Xia, T.; Wu, W.; Zhou, Q.; Zhou, Y. Comparison of two inversion methods for winter wheat leaf area index based on hyperspectral remote sensing. *Trans. Chin. Soc. Agric. Eng. (Trans. CSAE)* **2013**, *29*, 139–147. (In Chinese with English Abstract)
27. Gu, H.; Mills, C.; Ritchie, G.L.; Guo, W. Water Stress Assessment of Cotton Cultivars Using Unmanned Aerial System Images. *Remote Sens.* **2024**, *16*, 2609. [CrossRef]
28. Gitelson, A.A.; Gritz, Y.; Merzlyak, M.N. Relationships between Leaf Chlorophyll Content and Spectral Reflectance and Algorithms for Non-Destructive Chlorophyll Assessment in Higher Plant Leaves. *J. Plant Physiol.* **2003**, *160*, 271–282. [CrossRef]
29. Zheng, H.; Li, W.; Jiang, J.; Liu, Y.; Cheng, T.; Tian, Y.; Zhu, Y.; Cao, W.; Zhang, Y.; Yao, X. A Comparative Assessment of Different Modeling Algorithms for Estimating Leaf Nitrogen Content in Winter Wheat Using Multispectral Images from an Unmanned Aerial Vehicle. *Remote Sens.* **2018**, *10*, 2026. [CrossRef]
30. Sripada, R.P.; Heiniger, R.W.; White, J.G.; Meijer, A.D. Aerial Color Infrared Photography for Determining Early In-Season Nitrogen Requirements in Corn. *Agron. J.* **2006**, *98*, 968–977. [CrossRef]
31. Liu, J.; Zhu, Y.; Song, L.; Su, X.; Li, J.; Zheng, J.; Zhu, X.; Ren, L.; Wang, W.; Li, X. Optimizing Window Size and Directional Parameters of GLCM Texture Features for Estimating Rice AGB Based on UAVs Multispectral Imagery. *Front. Plant Sci.* **2023**, *14*, 1284235. [CrossRef]
32. Kou, J.; Duan, L.; Yin, C.; Ma, L.; Chen, X.; Gao, P.; Lv, X. Predicting Leaf Nitrogen Content in Cotton with UAV RGB Images. *Sustainability* **2022**, *14*, 9259. [CrossRef]
33. Han, Y.; Zhang, J.; Bai, Y.; Liang, Z.; Guo, X.; Zhao, Y.; Feng, M.; Xiao, L.; Song, X.; Zhang, M.; et al. Ensemble Learning-Driven and UAV Multispectral Analysis for Estimating the Leaf Nitrogen Content in Winter Wheat. *Agronomy* **2025**, *15*, 1621. [CrossRef]
34. Zhou, X.; Yang, M.; Chen, X.; Ma, L.; Yin, C.; Qin, S.; Wang, L.; Lv, X.; Zhang, Z. Estimation of Cotton Nitrogen Content Based on Multi-Angle Hyperspectral Data and Machine Learning Models. *Remote Sens.* **2023**, *15*, 955. [CrossRef]
35. Li, H.; Huang, C.; Zhang, Y.; Li, S.; Liu, Y.; Yang, K.; Lu, J. Estimating Maize Leaf Area Index Using Multi-Source Features Derived from UAV Multispectral Imagery and Machine Learning Models. *Plants* **2025**, *14*, 3534. [CrossRef]
36. Castilho Silva, D.; Emoke Madari, B.; Santana Carvalho, M.D.C.; Ferreira, M.E. Optimizing Nitrogen Estimates in Common Bean Canopies throughout Key Growth Stages via Spectral and Textural Data from Unmanned Aerial Vehicle Multispectral Imagery. *Eur. J. Agron.* **2025**, *169*, 127697. [CrossRef]
37. Fan, Y.; Feng, H.; Yue, J.; Jin, X.; Liu, Y.; Chen, R.; Bian, M.; Ma, Y.; Song, X.; Yang, G. Using an Optimized Texture Index to Monitor the Nitrogen Content of Potato Plants over Multiple Growth Stages. *Comput. Electron. Agric.* **2023**, *212*, 108147. [CrossRef]
38. Hu, S.; Bao, Y.L.; Tubuxinbayaer; Tao, J.F.; Guo, E.L. Chlorophyll Content Inversion of Spring Wheat Based on Unmanned Aerial Vehicle Hyperspectral and Integrated Learning. *J. Agric. Sci. Technol.* **2025**, *27*, 93–103. (In Chinese with English Abstract) [CrossRef]

Disclaimer/Publisher's Note: The statements, opinions and data contained in all publications are solely those of the individual author(s) and contributor(s) and not of MDPI and/or the editor(s). MDPI and/or the editor(s) disclaim responsibility for any injury to people or property resulting from any ideas, methods, instructions or products referred to in the content.